Gogny-Hartree-Fock-Bogolyubov plus quasiparticle random-phase approximation predictions of the $M1$ strength function and its impact on radiative neutron capture cross section

S. Goriely,[1] S. Hilaire,[2] S. Péru,[2] M. Martini,[3] I. Deloncle,[2,4] and F. Lechaftois[2]
[1]*Institut d'Astronomie et d'Astrophysique, Université Libre de Bruxelles, CP-226, 1050 Brussels, Belgium*
[2]*CEA, DAM, DIF, F-91297 Arpajon, France*
[3]*ESNT, CEA, IRFU, Service de Physique Nucléaire, Université de Paris-Saclay, F-91191 Gif-sur-Yvette, France*
[4]*CSNSM, CNRS and Université Paris-Sud, F-91405 Orsay Campus, France*

(Received 26 July 2016; published 7 October 2016)

Valuable theoretical predictions of nuclear dipole excitations in the whole chart are of great interest for different nuclear applications, including in particular nuclear astrophysics. Here we extend our large-scale calculations of the $E1$ γ-ray strength function, obtained in the framework of the axially- symmetric-deformed quasiparticle random phase approximation (QRPA) based on the finite-range D1M Gogny force, to the calculation of the $M1$ strength function. We compare our QRPA prediction of the $M1$ strength with available experimental data and show that a relatively good agreement is obtained provided the strength is shifted globally by about 2 MeV and increased by an empirical factor of 2. Predictions of the $M1$ strength function for spherical and deformed nuclei within the valley of β stability as well as in the neutron-rich region are discussed. Its impact on the radiative neutron capture cross section is also analyzed.

DOI: 10.1103/PhysRevC.94.044306

I. INTRODUCTION

Radiative neutron capture cross sections play a key role in almost all nuclear applications. Despite a huge effort to measure such radiative neutron capture cross sections, theoretical predictions are required to fill the gaps, both for nuclei for which measurements are not feasible at the present time, in particular for unstable targets, and for energies that cannot be reached in the laboratory. Some applications, such as nuclear astrophysics, also require the determination of radiative neutron capture cross sections for a large number of exotic neutron-rich nuclei [1]. In this case, large-scale calculations on the basis of sound and accurate models need to be performed to ensure a reliable extrapolation far away from the experimentally known region.

The neutron capture rates are commonly evaluated within the framework of the statistical model of Hauser-Feshbach, although the direct capture contribution plays an important role for very exotic nuclei [2]. The fundamental assumption of the Hauser-Feshbach model is that the capture goes through the intermediary formation of a compound nucleus in thermodynamic equilibrium. In this approach, the (n,γ) cross section strongly depends on the electromagnetic interaction, i.e., the photon deexcitation probability. In turn, it is well known that the photon strength function is dominated by the electric dipole contribution. The various multipolarities of the γ-ray strength function are traditionally modeled by the phenomenological Lorentzian approximation or some of its energy-dependent variants [3]. The reliability of the γ-ray strength predictions can, however, be greatly improved by the use of microscopic or semimicroscopic models. Indeed, provided satisfactory reproduction of available experimental data, the more microscopic the underlying theory, the greater the confidence in the extrapolations out towards the experimentally unreachable regions. Microscopic approaches are rarely used for practical applications essentially for two reasons. First, the time cost is often prohibitive for large-scale calculations. Second, the fine tuning required to reproduce accurately a large experimental data set is very delicate, in addition to being time consuming. A prominent exception is represented by Refs. [4–6] where a complete set of γ-ray strength functions was derived from mean field plus quasiparticle random-phase approximation (QRPA) calculations. In Refs. [4,5], zero-range Skyrme forces were considered and phenomenological corrections applied to properly describe the splitting of the giant dipole resonance in deformed nuclei as well as the damping of the collective motion.

Recently, axially-symmetric-deformed QRPA calculations based on Hartree-Fock-Bogoliubov (HFB) calculations using the finite-range Gogny interaction have been shown to provide rather satisfactory predictions of the $E1$ strength [6]. Such calculations have been used to estimate the corresponding radiative neutron capture cross sections. However, the contribution of the other multipolarities is still calculated on the basis of standard Lorentzian-type functionals that have been parametrized on the few experimental data available. Among those, the $M1$ strength is known to dominate after the $E1$ contribution. The magnetic dipole response is known experimentally to include two major components, namely (i) an orbital component at low excitation energies, typically around 3 MeV, which in deformed nuclei is called the scissors mode [7], and (ii) a spin-flip component around 8 MeV which includes the largest fraction of the $M1$ strength. The scissors mode in deformed nuclei is interpreted as neutrons and protons vibrating with a small angle with respect to each other in a scissors-like motion, while the higher energy component describes a resonance-like structure made of proton and neutron spin-flip excitations. Theoretical as well as experimental insights on the magnetic dipole excitations in nuclei can be found in the review paper of Ref. [8].

In the present paper, we complement our previous study of the $E1$ strength [6], as well as of the charge exchange

Gamow-Teller strength [9], by estimating the magnetic dipole $M1$ strength within exactly the same HFB+QRPA framework on the basis of the same D1M interaction [10]. QRPA calculations of the $M1$ strength have been performed in the past (see, e.g., Refs. [11–14]). The present calculations has, however, the specificity to have been applied to a large number of nuclei, to be based on the finite-range Gogny interaction, and, most of all, to be axially-symmetric deformed. The latter property consequently allows us to estimate also the scissors component of the $M1$ strength. Due to the scarcity of experimental data in the giant resonance region, i.e. around 8–9 MeV, the QRPA prediction provides an alternative way with respect to the phenomenological standard Lorentzian (SLO) description of the spin-flip giant resonance mode [3] to estimate the $M1$ contribution for a large set of nuclei. In addition, it is also well known that the low-energy scissors mode for deformed nuclei is not described by the Lorentzian approximation. In this case, a more microscopic model can provide some systematic insight of its amplitude and its impact on the total strength function and consequently on the radiative capture cross section.

The paper is organized as follows. In Sec. II, the axially-symmetric-deformed HFB+QRPA formalism is described in its standard form and the way corrections beyond QRPA are included phenomenologically is detailed. The QRPA prediction of the $M1$ strength function is discussed in Sec. III, including its sensitivity to the size of the finite harmonic oscillator (HO) basis and the cutoff effects. In Sec. IV, we compare our D1M+QRPA prediction of the $M1$ strength with available experimental data, and, in Sec. V, we study the $M1$ strength function in exotic neutron-rich nuclei. The impact of the newly calculated $M1$ strength function on the Hauser-Feshbach estimate of the radiative neutron capture cross section is discussed in Sec. VI. Conclusions are finally drawn in Sec. VII.

II. THE THEORETICAL MODEL

A. Standard HFB+QRPA approach

We summarize here the formalism of the consistent QRPA approach based on axially-symmetric-deformed HFB equations solved in a finite HO basis in cylindrical coordinate. For more details, we refer the reader to Refs. [6,15–17]. In the present calculation, the number of involved major shells is $N_{\rm sh} = N_0 + 1$ where N_0 is the maximum value of the energy quantum number N. Solving the HFB equations in an HO basis leads to the diagonalization of an Hamiltonian matrix: eigenvalues and eigenvectors are respectively Bogoliubov quasiparticle (qp) excitation energies and u and v components of the Bogoliubov transformation. As a consequence the positive energy continuum is discretized. The first-order excitations for even-even nuclei are given by two-quasiparticle (2-qp) excitations. QRPA phonons are linear combinations of these 2-qp excitations. According to the symmetries imposed, the projection K of the angular momentum J on the symmetry axis and the parity Π are good quantum numbers for the phonons. Consequently, QRPA calculations can be performed separately for each K^Π set. In this context, phonons are characterized by the excitation operator

$$\theta^+_{n,K^\Pi} = \sum_{ij} X^{ij}_{n,K^\Pi}\eta^+_i\eta^+_j - (-)^K Y^{ij}_{n,K^\Pi}\eta_j\eta_i, \tag{1}$$

where η^+ and η are the qp operators, related to the HO particle operators c^+ and c through the u and v Bogoliubov transformation matrices:

$$\eta^+_i = u_{i\alpha}c^+_\alpha - v_{i\alpha}c_\alpha. \tag{2}$$

Here and in the following, repeated indices are implicitly summed over; latin and greek letters denote qp and harmonic oscillator states, respectively. In principle QRPA calculation can be performed without any cut-off in energy of the 2-qp states neither in occupation probabilities (v^2) of single-qp states. The amplitudes X and Y of Eq. (1) are solutions of the well-known QRPA matrix equation [18]

$$\begin{pmatrix} A & B \\ B & A \end{pmatrix}\begin{pmatrix} X_{n,K^\Pi} \\ Y_{n,K^\Pi} \end{pmatrix} = \omega_{n,K^\Pi}\begin{pmatrix} X_{n,K^\Pi} \\ -Y_{n,K^\Pi} \end{pmatrix}, \tag{3}$$

where $\omega_{n,K}$ are the energies of the QRPA excited states. To ensure consistency, the same interaction (parameter set of the Gogny force) is used to calculate the A and B matrix elements and the underlined HFB mean field [16]. In the present study, we consider the D1M [10] Gogny force only. Once the QRPA matrix is diagonalized, the X and Y amplitudes allow to calculate the strength for each electromagnetic mode. Here, we focus on the magnetic dipole (multipolarity $\lambda = 1$, parity $\Pi = +$) mode. The corresponding excitation operator is

$$\hat{T}_{1,K} = \mu_N\sqrt{\frac{3}{4\pi}}\sum_i^A \left(g_l^{(i)}(l_K)_i + g_s^{(i)}(s_K)_i\right), \tag{4}$$

where μ_N is the Bohr magneton and g_l and g_s the orbital and spin gyromagnetic factors for which we take the free-nucleon values, i.e.,

$$g_l^{(i)} = 1, \quad g_s^{(i)} = 5.586 \quad \text{for protons,}$$
$$g_l^{(i)} = 0, \quad g_s^{(i)} = -3.826 \quad \text{for neutrons.}$$

Note that no quenching is applied to the g_s factor. We remind here of the correspondence $\{0,1,-1\} \leftrightarrow \{z,+,-\}$ between the K values and the components of the spin and angular momentum operators.

The total magnetic distribution $B(M1)$ (in μ_N^2) is obtained by summing the contributions of $K^\Pi = 0^+$ and twice that of $K^\Pi = 1^+$, the $K^\Pi = -1^+$ solution being equal to the $K^\Pi = 1^+$ one through the conservation of time reversal symmetry. We remind that in the spherical symmetry case, the $K = 0$ and $|K| = 1$ states are degenerate. In deformed nuclei, the strength splits up into two components corresponding to two different angular momentum projection K values.

B. Beyond the QRPA description

The well established formalism described above takes into account only 2-qp excitations. Meson-exchange currents and Δ-isobar excitations effects [19] are not included in the present approach. Furthermore, more complex excitations than the simple 2-qp ones are not taken into account. As discussed in

Ref. [20], multiparticle multihole effects increase significantly the orbital part of the magnetic transition operator. The interaction between the single-particle and low-lying collective phonon degrees of freedom [21] leads to a fragmentation and broadening of the response and to a dynamical redistribution of the transition strength by shifting part of the strength. To include all the aforementioned ingredients beyond the 2-qp excitations in a phenomenological way, the discrete QRPA $B(M1)$ distribution is folded by a Lorentzian function

$$L(E,\omega) = \frac{1}{\pi}\frac{\Gamma E^2}{[E^2-(\omega-\Delta)^2]^2+\Gamma^2 E^2}, \quad (5)$$

leading to a continuous $M1$ strength function

$$S_{M1}(E) = f_{\rm corr} \times \sum_n L(E,\omega_n) B(M1)(\omega_n). \quad (6)$$

Then, the $M1$ strength function f_{M1} (in MeV^{-3}) can be deduced from S_{M1} by applying the conversion factor of 0.044 (e.g., [22]).

In Eq. (5), Γ is the width at half maximum and Δ allows for an energy shift. For the $E1$ strength function, these quantities have been adjusted on experimental photoabsorption data. In the present study, similar corrections are applied to the $M1$ resonance, at least in the zero-order approximation (the so-called Model 0 in Ref. [6]). For the $M1$ component, we adopt a similar shift of $\Delta = 2$ MeV for the spin-flip resonance; however, such a shift at and above the centroid energy of 10 MeV can hardly be applied to the $M1$ strength at the lowest energies, in particular to the scissors mode in deformed nuclei. A study of our QRPA predictions of the low-energy vibrational states shows that the first experimental energies [23] are overestimated by typically 500 keV. For this reason, we apply in the present study an energy shift of $\Delta = 0.5$ MeV for $E \leqslant 0.5$ MeV and $\Delta = 2$ MeV for $E \geqslant 10$ MeV, and for $0.5 \leqslant E \leqslant 10$ MeV, the energy shift Δ is interpolated linearly between these two values. This shift describes in a very approximate way the energy-dependent effects beyond the standard 2-qp QRPA excitations and the coupling between the single-particle and low-lying collective phonon degrees of freedom. This approximation represents a simplified version of Models 1 or 2 in Ref. [6], where the energy-dependence was assumed to be proportional to the density of four quasiparticles.

As far as the broadening is concerned, in order to keep some structure inherent to the QRPA calculation, we adopt a width $\Gamma = 0.5$ MeV. Indeed, considering a larger width of 2.5 MeV, as used in Model 0 of Ref. [6] and required to reproduce the dominant $E1$ component of the giant resonance properties seen in photoabsorption data, would inevitably wipe out most of the structure, in particular at low energies where a non-negligible part of the strength is located, especially for deformed nuclei.

Finally, the correction factor of $f_{\rm corr} = 2$ is applied in Eq. (6) to reproduce at best measured $M1$ strengths, as discussed in Sec. IV. Note that the $B(M1)$ distributions have not been calculated for odd-A and odd-odd nuclei. To estimate their $M1$ strength, we have used the same interpolation procedure as the one used for the $E1$ strength (see Ref. [6] for more details).

III. THE QRPA PREDICTION OF THE $M1$ STRENGTH FUNCTION

The HFB+QRPA calculations remain sensitive to the number of HO shells used and the energy cutoff E_c accounted for on the 2-qp state energies. Below we discuss the impact of these effects on the calculated $M1$ strength function, keeping in mind the feasibility of such calculations regarding computational constraints.

A. Sensitivity analysis

A key ingredient of any QRPA calculation concerns the number of HO shells, $N_{\rm sh}$, included, as well as the cutoff energy E_c on the 2-qp states energies. In order to investigate the impact of $N_{\rm sh}$ on the γ-ray strength function and to verify the convergence, we have performed QRPA calculations for several odd values of $N_{\rm sh}$ and different energy cutoffs. The results are shown in Fig. 1 where the QRPA strength is widened by a Lorentzian function Eq. (5) of width of $\Gamma = 0.5$ MeV, no shift being applied ($\Delta = 0$). It can be seen that the $M1$ strength distribution remains rather insensitive to the cutoff energy, only the high-energy spin-flip resonance may be shifted upward by a few hundred keV if a small energy cutoff of 60 MeV is adopted. Similarly, the $M1$ strength function is not too much affected by the size of the HO basis. A low value of $N_{\rm sh}$ is seen to affect the high-energy resonance, but otherwise the strength distribution

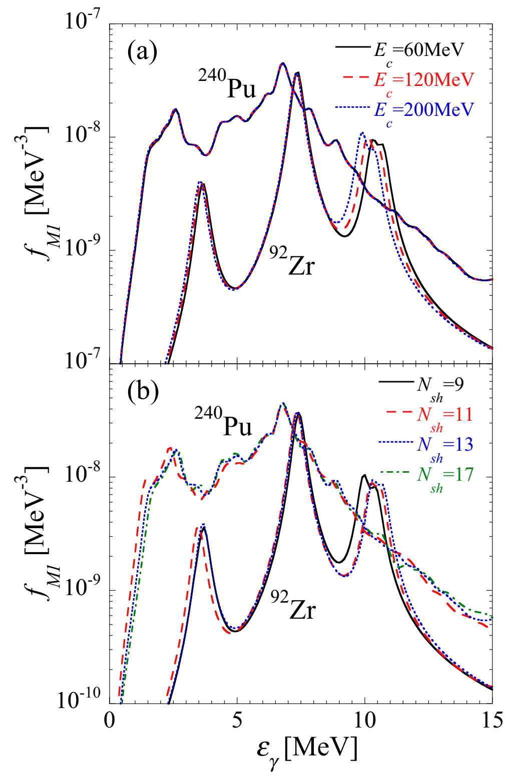

FIG. 1. (a) $M1$ strength f_{M1} for ^{92}Zr and ^{240}Pu for a number of HO shells $N_{\rm sh} = 13$ and different cutoff energies $E_c = 60$, 120, and 200 MeV. (b) The same as (a) for $E_c = 60$ MeV and different shell numbers $N_{\rm sh} = 9$, 11, 13, and 17 (the case of $N_{\rm sh} = 17$ has been calculated in the Pu case only).

remains rather robust with respect to different adopted values of $N_{\rm sh}$. Clearly the differences shown in Fig. 1 have no impact of any kind on the radiative neutron capture cross section calculated in Sec. VI. For these reasons, most of the $M1$ calculations presented here have been obtained with a basis dimension of $N_{\rm sh} \geqslant 11$ and a cutoff energy of $E_c = 60$ MeV (for N and $Z \leqslant 70$, we adopt $N_{\rm sh} \geqslant 9$).

B. The QRPA $M1$ strength

The $B(M1)$ strength has been calculated for about 412 even-even nuclei from O to Pu including the valley of β stability as well as neutron-rich nuclei with $26 \leqslant Z \leqslant 70$ and up to around 20 extra neutrons away from the valley of stability (for Sn, the calculation includes isotopes up to the neutron drip line). The corresponding centroid energies and total integrated strengths are shown in Fig. 2. It can be seen that the centroid energy systematically lies between 10 and 12 MeV with some peak structure observed around neutron magic numbers. In such spherical nuclei, no scissors mode is obtained, so that the strength is not brought down to lower energies, as in deformed nuclei. The integrated strength is found to increase significantly as a function of the atomic

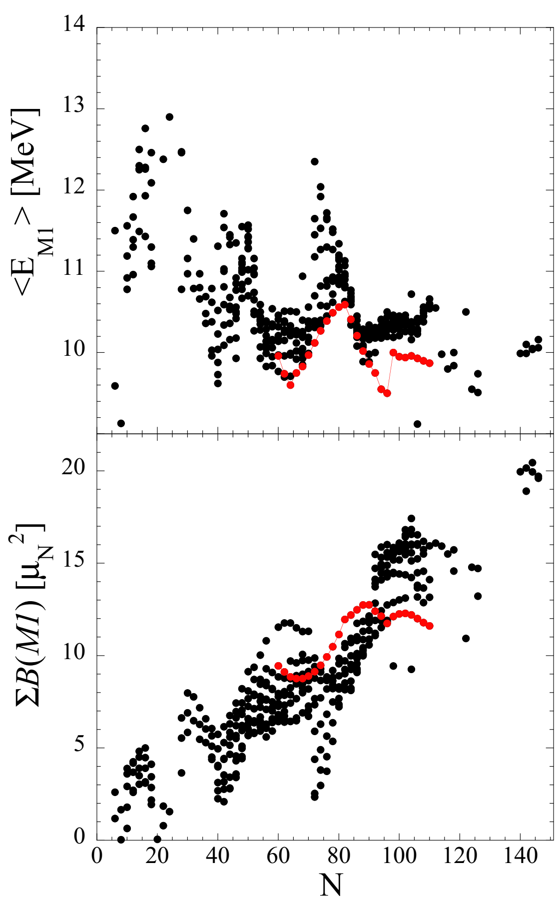

FIG. 2. Centroid $M1$ energy and total $B(M1)$ strength estimated for the 412 even-even nuclei around the valley of stability for which QRPA calculations have been performed. The Sn isotopic chain is shown by the red circles.

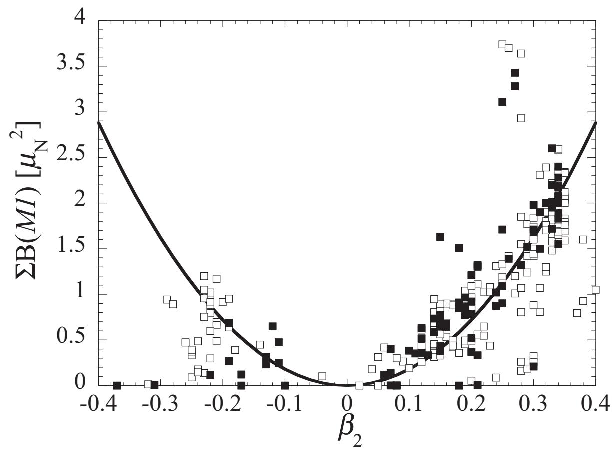

FIG. 3. Total $K = 1^+$ strength below 4.5 MeV as a function of the quadrupole deformation β_2 for the deformed nuclei in our set of 412 even-even nuclei. The full squares correspond to stable nuclei and long-lived actinides, while open squares depict neutron-rich nuclei. The solid curve is the $18\beta_2^2$ function in μ_N^2 units.

mass and the neutron number, although we find that for the Sn isotopic chain it saturates to a rather constant value within the neutron rich region for $N \gtrsim 88$.

In Fig. 3, we show for deformed nuclei the total $K = 1^+$ strength obtained below 4.5 MeV as a function of the quadrupole deformation β_2. The strength of the corresponding scissors mode is found to globally increase as the square of the deformation, as already pointed out in Ref. [8] on the basis of experimental data in the rare earth region. The overall quadratic dependence $18\beta_2^2$ is about twice lower than found experimentally, justifying the need to increase the QRPA strength by a factor $f_{\rm corr}$ of about 2, as discussed in Sec. IV. It should be noted that a strict energy threshold at 4.5 MeV captures most of the strength in the scissors mode but remains an approximation. The actinides with a significant strength above $3\mu_N^2$ are seen not to follow the global trend. A set of nuclei are also characterized with a scissors mode strength about twice smaller; they are, essentially, neutron-rich isotopes of Kr, Te, and Hg. Similarly, some light stable isotopes of Mg and Si do not present any significant low-energy $M1$ strength.

IV. COMPARISON WITH EXPERIMENTAL DATA

In this section, we compare our D1M+QRPA prediction of the $M1$ strength S_{M1} after renormalization by the $f_{\rm corr}$ factor and the energy shift Δ with available experimental data. The first comparison is shown in Fig. 4 for ^{106}Pd and ^{198}Au which represent two cases where the giant $M1$ strength has been derived experimentally from a detailed analysis of the average resonance capture data [24–26]. As can be observed, the strength around the spin-flip resonance mode between 6 and 8 MeV for ^{106}Pd and 4 to 6 MeV for ^{198}Au is relatively well described by the QRPA calculation. In addition to the main strength in this region, some D1M+QRPA $M1$ strength is predicted at low energies, around 3 MeV, corresponding to the scissors mode for the ^{106}Pd deformation of $\beta_2 = 0.19$ found with the D1M interaction. ^{198}Au is predicted to be oblate with a

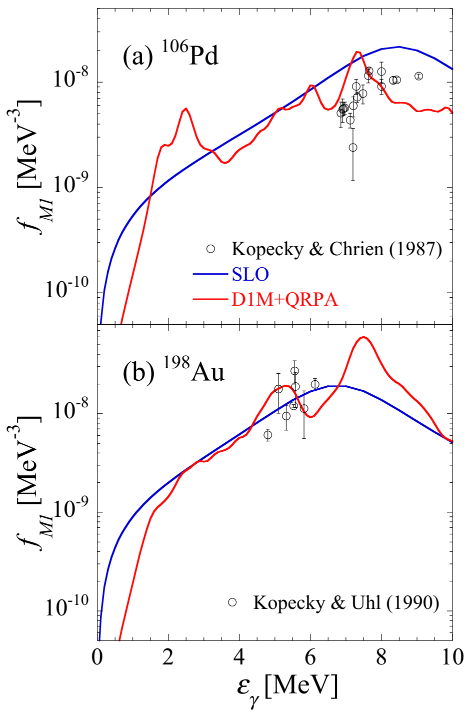

FIG. 4. (a) Comparison between experimental [24,25] and D1M+QRPA $M1$ strength functions for ^{106}Pd. Also shown is the SLO approximation recommended in Ref. [27]. (b) The same for ^{198}Au with experimental data taken from [24,26].

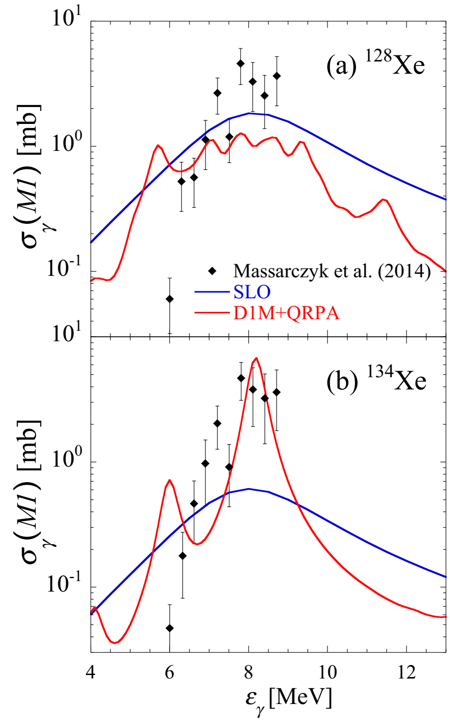

FIG. 5. Same as Fig. 4 for the $M1$ photoabsorption cross section σ_γ of (a) ^{128}Xe and (b) ^{134}Xe. Experimental data are taken from Ref. [28].

small deformation of $\beta_2 = -0.11$ and its D1M+QRA strength does not show a significant contribution at low energies, but rather around 8 MeV. Keeping in mind that the strength function of this odd-odd nucleus is obtained by interpolation, blocking approximation would further improve its calculation.

We also compare in Fig. 4 the global phenomenological model recommended by the RIPL-1 library [27]. In this case, the $M1$ strength function is assumed to be described by the spin-flip giant resonance mode through a SLO function

$$f_{M1}^{\mathrm{SLO}}(\varepsilon_\gamma) = \frac{\sigma_0}{3(\pi\hbar c)^2}\frac{\varepsilon_\gamma\Gamma_0^2}{\left(\varepsilon_\gamma^2 - E_0^2\right)^2 + \varepsilon_\gamma^2\Gamma_0^2} \tag{7}$$

with a global parametrization for the centroid energy and width corresponding to $E_0 = 41A^{-1/3}$ MeV and $\Gamma_0 = 4$ MeV [3] and for a peak cross section such that, at the reference energy of 7 MeV, $f_{M1}^{\mathrm{SLO}} = 1.5810^{-9}A^{0.47}$ MeV^{-3} [27]. Other prescriptions for the amplitude of the $M1$ strength function have been proposed, in particular relating the $E1$ and $M1$ strengths around the same reference energy of 7 MeV through $f_{E1}/f_{M1} = 0.0588A^{0.878}$ [3], but will not be considered in the present study, since it remains sensitive to the adopted $E1$ strength model.

Similarly to Fig. 4, we compare in Fig. 5 the experimental $M1$ photoabsorption cross section of the slightly deformed ^{128}Xe and spherical ^{134}Xe obtained with quasimonoenergetic and linearly polarized γ-ray beams [28] with our D1M+QRPA predictions as well as the SLO prescription [27]. Although the $M1$ cross section in the energy region of the spin-flip resonance is underestimated and rather too broad for ^{128}Xe (resulting essentially from the deformation effects), the overall ^{134}Xe cross section is rather well described, especially in comparison with the SLO approximation. Similar QRPA results were obtained in Ref. [28].

Figure 6 compares the integrated experimental $M1$ strength estimated within a given energy range [29–39] with the one predicted by our D1M+QRPA model. Most of these ranges, especially for rare-earth and actinide nuclei, are located at low energies between typically 2 and 4 MeV and correspond to the scissors mode (they are shown as circles in Fig. 6). The integrated strength measured above $5\mu_N^2$ corresponds to

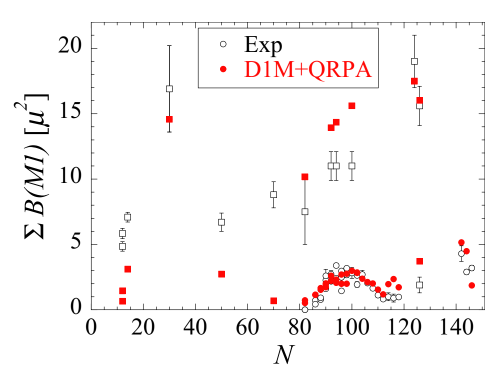

FIG. 6. Comparison between experimental [29–40] (open symbols) and D1M+QRPA (full symbols) values of the integrated strength $\sum B(M1)(\mu_N^2)$ in the well defined energy range given by the measurements. Circles and squares correspond to data below or above 4 MeV, respectively.

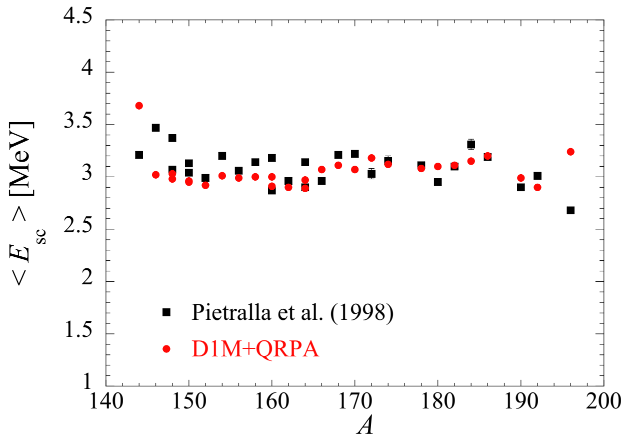

FIG. 7. Comparison between experimental [41] and D1M+QRPA mean excitation energy of the scissors mode.

energy ranges closer to the giant resonance mode above 4 MeV. Globally it can be seen that, with the correction factor of 2 and the 2 MeV shift introduced in the QRPA strength [Eq. (6)], the total strength observed is relatively well described, especially for the scissors mode. Similarly, the excitation of the scissors mode is found to be systematically located around 3 MeV for all rare-earth nuclei for which experimental data is available at low energies [8,41], as shown in Fig. 7. The D1M+QRPA mean energy

$$\langle E_{\rm sc}\rangle = \frac{\int_0^{E_{\rm max}} E S_{M1}(E)dE}{\int_0^{E_{\rm max}} S_{M1}(E)dE} \tag{8}$$

illustrated in Fig. 7 is obtained assuming the scissors mode lies below $E_{\rm max} = 4.5$ MeV, and is seen to reproduce fairly well the constant measured value, provided the energy shift Δ, as described in Sec. II B, is applied.

The need for an energy shift and scaling factor $f_{\rm corr}$ corrections to the D1M+QRPA strength is also confirmed when comparing our $B(M1)$ strength distribution in ^{208}Pb with experimental data between 7 and 9 MeV. We show in Fig. 8 our D1M+QRPA predictions with and without the energy shift

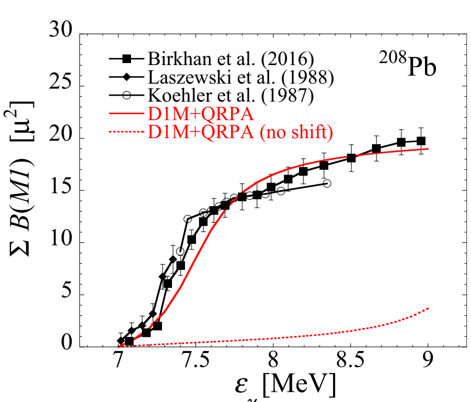

FIG. 8. Comparison between experimental [31,42,43] and D1M+QRPA integrated $M1$ strength in ^{208}Pb between 7 and 9 MeV with (solid line) and without (dashed line) energy shift Δ.

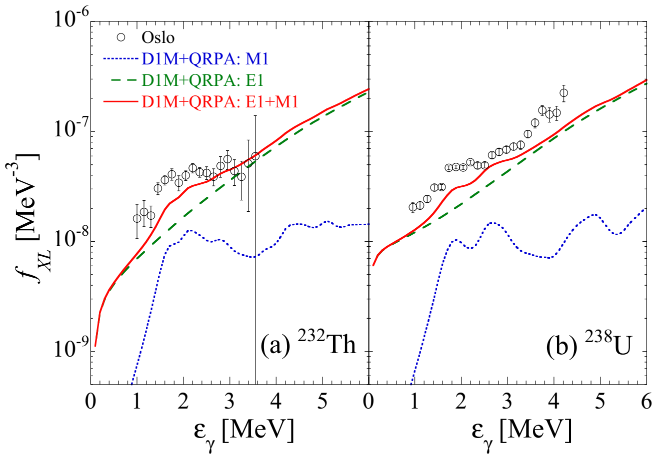

FIG. 9. (a) Comparison between experimental [44] and D1M+QRPA strength for ^{232}Th. The dotted, dashed, and solid lines correspond to the $M1$, $E1$, and total $E1+M1$ QRPA strengths, respectively. (b) The same for ^{238}U.

Δ and clearly experimental data can only be described when applying the energy shift. The same holds when comparing our predictions with the ^{232}Th and ^{238}U strengths deduced from the Oslo method [44], as illustrated in Fig. 9. However, in this case, the measured data also significantly depends on the dominant $E1$ component which for consistency has been estimated within the same D1M+QRPA approach [6]. Note however that the $E1$ strength in the deexcitation process might be affected by temperature effects and consequently be higher than predicted in the present zero-temperature QRPA case.

Important information on the $M1$ strength is also hidden in the total radiative width $\langle\Gamma_\gamma\rangle$ defined as

$$\langle\Gamma_\gamma\rangle = \frac{D_0}{2\pi}\sum_{X,L,J,\pi}\int_0^{S_n+E_n} T_{XL}(\varepsilon_\gamma) \tag{9}$$

$$\times\,\rho(S_n+E_n-\varepsilon_\gamma,J,\pi)d\varepsilon_\gamma, \tag{10}$$

where the summation includes all multipolarities (X,L) between all spins J and parities π in the electromagnetic cascade starting at the neutron energy E_n above the neutron separation energy S_n. In Eq. (10), D_0 is the s-wave neutron spacing at S_n and ρ the nuclear level density. Since the total radiative width is sensitive to all multipolarities and to nuclear level densities, it remains also affected by the $M1$ strength below the neutron separation energy. In deformed nuclei, the $M1$ scissors mode may contribute significantly, as already pointed out, e.g., in Ref. [45]. We show in Fig. 10 the total radiative width obtained within the D1M+QRPA approach, including both the $E1$ and $M1$ contributions, together with the experimental compilation [3]. The error bars on the D1M+QRPA predictions are obtained by considering different nuclear level density prescriptions [23,46,47]. While lower $\langle\Gamma_\gamma\rangle$ values are usually predicted for $A \lesssim 160$ nuclei, larger estimates are obtained above. However, globally, the total radiative widths are satisfactorily described despite the large uncertainties stemming from the level densities. The radiative width obtained by omitting totally the contribution of the $M1$

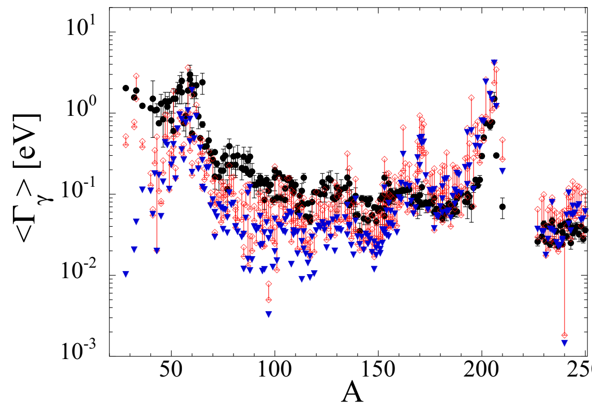

FIG. 10. Comparison between experimental (black dots) [3] and D1M+QRPA estimate of the $\langle\Gamma_\gamma\rangle$ value (open red diamonds) including both the $E1$ and $M1$ contributions. The theoretical uncertainties stem from the use of different nuclear level density prescriptions [23,46,47]. The blue triangles correspond to the predicted $\langle\Gamma_\gamma\rangle$ when omitting the $M1$ mode totally.

mode is also illustrated in Fig. 10 using the combinatorial level density model of Ref. [46]. This calculation illustrates the significant contribution of the $M1$ strength in the $A < 160$ region.

V. EXTRAPOLATION TO NEUTRON-RICH NUCLEI

The $M1$ strength function for the Ni and Sn isotopic chains are shown in Fig. 11. For the spherical Ni and $^{120-144}$Sn isotopes, the strength is essentially characterized by two main peaks, one located around 5 MeV and the upper one between 8 and 11 MeV depending on the neutron richness. Such a double peak structure has been confirmed experimentally in the spherical stable ^{58}Ni isotope [40]. Only the doubly magic ^{132}Sn strength is single peaked. A secondary low-energy peak also starts to emerge around 2–3 MeV for the spherical $^{80-84}$Ni and $^{136-144}$Sn neutron-rich nuclei; such a low-energy strength is not present in spherical nuclei close to the valley of β stability. For the deformed $^{148-160}$Sn isotopes, an important strength from the scissors mode is found to be located systematically around 2.5–3 MeV, regardless of the neutron richness. In this case, the strength is essentially distributed between 2.5 and 10 MeV with a four peak structure.

VI. IMPACT ON THE RADIATIVE NEUTRON CAPTURE CROSS SECTION

The Maxwellian-averaged neutron capture cross section (MACS) has been systematically estimated, on the basis of the TALYS code [48–50], for the 1400 nuclei for which the $M1$ and $E1$ strengths have been evaluated within the present D1M+QRPA approach. The absolute $M1$ contribution to the MACS has been obtained by comparing with a similar calculation where the $M1$ component has been totally neglected. The impact of the $M1$ strength is illustrated in Fig. 12. In many nuclei, especially deformed ones where the low-energy scissors mode is present, the $M1$ contribution is found to amount to 20% or more. In light $Z \simeq N \lesssim 18$ nuclei,

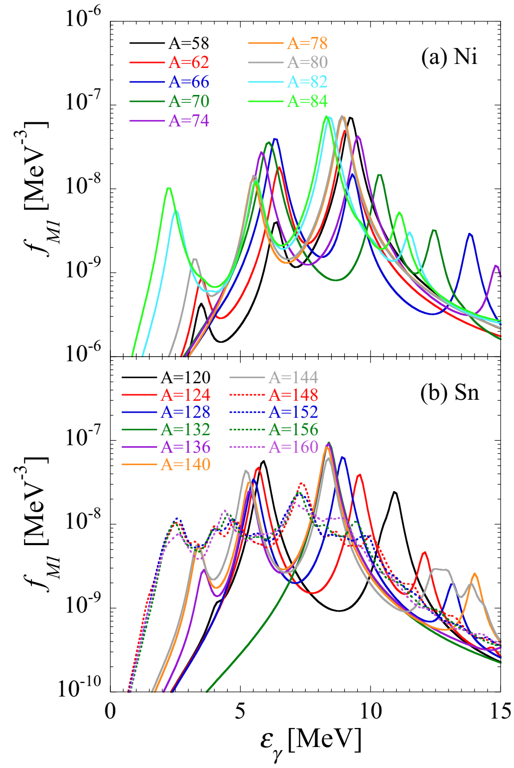

FIG. 11. (a) D1M+QRPA $M1$ strength function in the Ni isotopic chain. (b) The same for the Sn isotopic chain. Spherical nuclei are shown with solid lines and deformed ones with dotted lines.

as well as neutron-rich isotopes of Cr, Mn, or Fe, the $M1$ deexcitation mode is even found to strongly dominate with a contribution larger than 50%. In actinides, it contributes to some 20–30% of the MACS.

So far, most of the radiative capture cross sections have been calculated assuming the $M1$ giant resonance strength is described by a SLO function as the one given in Eq. (7) [3,27].

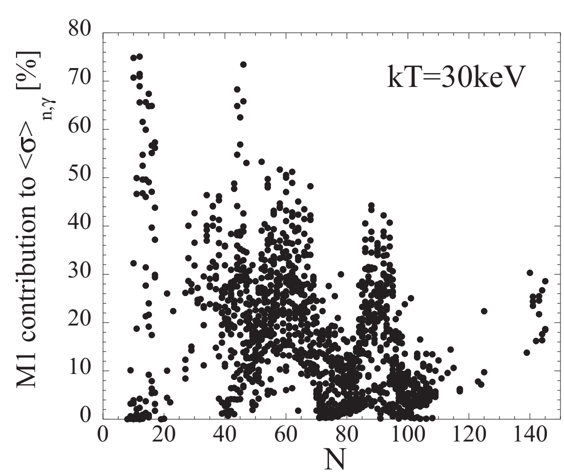

FIG. 12. Contribution (in %) of the D1M+QRPA $M1$ strength function to the total MACS for 1400 nuclei at the energy of $kT = 30$ keV.

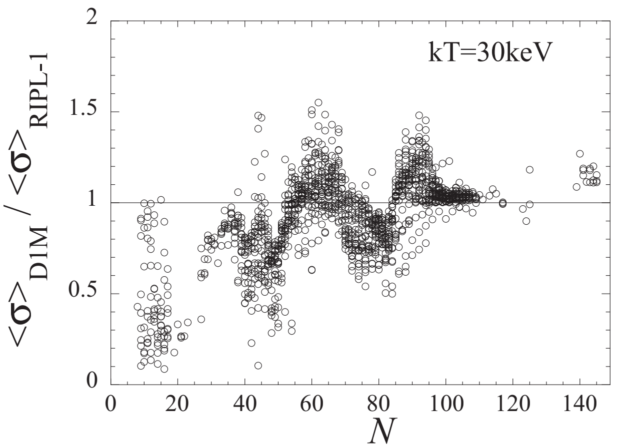

FIG. 13. Ratio of the MACS obtained with the D1M+QRPA $M1$ strength to the one obtained with the RIPL-1 recommendation [Eq. (7)] [27] for the 1400 nuclei at the energy of $kT = 30$ keV.

Such an approximation does not take into account the presence of the scissors mode at low energies in deformed nuclei and remains very schematic concerning the spreading of the strength around the centroid value. The pattern obtained within D1M+QRPA is significantly more complex, as shown in Fig. 11 and may consequently impact the radiative capture cross section. To illustrate such an impact, we show in Fig. 13 the ratio of the 30 keV MACS obtained with the D1M+QRPA $M1$ strength to the one obtained with the RIPL-1 recommendation [Eq. (7)] [27] for the same 1400 nuclei. For light nuclei as well as spherical nuclei in the vicinity of the neutron magic numbers, D1M+QRPA strength gives a lower cross section up to a factor of about 10; this is partially due to the wide broadening of the prescription in Eq. (7) with a width $\Gamma = 4$ MeV to be compared to the adopted value of $\Gamma = 0.5$ MeV which concentrates more strength around the centroid energy for spherical cases. For open shell nuclei a MACS larger by about 50% can be obtained. For actinides, the $M1$ contribution is also found to affect the MACS by about 10–30% through the low-energy scissors mode absent from the SLO description [27].

VII. CONCLUSIONS

Our large-scale calculations of the $E1$ γ-ray strength function in the framework of the axially-symmetric-deformed QRPA based on the finite-range D1M Gogny force has been extended to the $M1$ mode. This approach is applied to some 412 even-even nuclei, the strength function for odd nuclei being deduced by interpolation. To take into account for missing strength as well as effects beyond the 2-qp excitations, it has been necessary to include an energy shift ranging between 0.5 and 2 MeV as well as an increase of the global strength by a factor of 2. Provided such corrections are applied, our D1M+QRPA $M1$ strength appears to describe relatively well available experimental data. These include measured strengths in the spin-flip giant resonance region as well as integrated strengths at low energies. In particular, it is shown that the D1M+QRPA strength embodied in the scissors mode for deformed nuclei increases quadratically with deformation, is located around 3 MeV and rather well describes experimental data. The total radiative width is also found to be better described when calculated within the QRPA approach, essentially due to a proper description of the low-energy strength stemming from the scissors mode.

The D1M+QRPA $M1$ strength has also been estimated for neutron-rich nuclei far away from the valley of β stability. It is found that the scissors mode in deformed nuclei remains rather unaffected by the neutron richness, in contrast to the spin-flip resonance centroid energy. Some extra low-lying strength is also found to appear in exotic neutron-rich spherical nuclei. The $M1$ contribution to the radiative neutron capture cross section in the keV region can be significant, especially in light and deformed nuclei, but when compared with standard Lorentzian-type prescriptions, the QRPA predictions only affects the radiative neutron capture cross section within roughly 50%. The present QRPA prediction provides an alternative accurate and reliable way to estimate the $M1$ contribution for a large set of nuclei with respect to the phenomenological and approximate Lorentzian-type description of the spin-flip giant resonance mode [3].

ACKNOWLEDGMENTS

We gratefully thank A. Richter for valuable comments, J. Kopecky for providing us with updated ARC data, and T. Kawano and R. Capote for stimulating discussions. We acknowledge PRACE for awarding us access to resource CURIE based in FRANCE at TGCC-CEA. S.G. acknowledges the support of the FRS-FNRS (Belgium) and MM of the "Espace de Structure et de réactions Nucléaire Théorique" at CEA (France). This work was performed within the IAEA CRP on "Updating the Photonuclear data Library and generating a Reference Database for Photon Strength Functions" (F410 32).

[1] M. Arnould, S. Goriely, and K. Takahashi, Phys. Rep. **450**, 97 (2007).
[2] Y. Xu, S. Goriely, A. J. Koning, and S. Hilaire, Phys. Rev. C **90**, 024604 (2014).
[3] R. Capote *et al.*, Nucl. Data Sheets **110**, 3107 (2009).
[4] S. Goriely and E. Khan, Nucl. Phys. A **706**, 217 (2002).
[5] S. Goriely, E. Khan, and M. Samyn, Nucl. Phys. A **739**, 331 (2004).
[6] M. Martini, S. Péru, S. Hilaire, S. Goriely, and F. Lechaftois, Phys. Rev. C **94**, 014304 (2016).
[7] D. Bohle, A. Richter, W. Steffen, A. E. L. Dieperink, N. Lo Iudice, F. Palumbo, and O. Scholten, Phys. Lett. B **137**, 27 (1984).
[8] K. Heyde, P. von Neumann-Cosel, and A. Richter, Rev. Mod. Phys. **82**, 2365 (2010).
[9] M. Martini, S. Péru, and S. Goriely, Phys. Rev. C **89**, 044306 (2014).

[10] S. Goriely, S. Hilaire, M. Girod, and S. Péru, Phys. Rev. Lett. **102**, 242501 (2009).
[11] D. Zawischa, M. Macfarlane, and J. Speth, Phys. Rev. C **42**, 1461 (1990).
[12] D. Zawischa and J. Speth, Phys. Lett. B **252**, 4 (1990).
[13] P. Sarriguren, E. Moya de Guerra, R. Nojarov, and A. Faessler, J. Phys. G **19**, 291 (1993).
[14] R. R. Hilton, W. Höhenberger, and P. Ring, Eur. Phys. J. A **1**, 257 (1998).
[15] S. Péru and H. Goutte, Phys. Rev. C **77**, 044313 (2008).
[16] S. Péru and M. Martini, Eur. Phys. J. A **50**, 88 (2014).
[17] I. Deloncle, S. Péru, and M. Martini, Eur. Phys. J. A (to be published).
[18] P. Ring and P. Schuck, *The Nuclear Many-Body Problem* (Springer, New York, 1980).
[19] I. S. Towner and F. C. Khanna, Nucl. Phys. A **399**, 334 (1983).
[20] G. Rusev, N. Tsoneva, F. Donau, S. Frauendorf, R. Schwengner *et al.*, Phys. Rev. Lett. **110**, 022503 (2013).
[21] S. P. Kamerdzhiev and V. N. Tkachev, Phys. Lett. B **142**, 225 (1984).
[22] S. Nakayama, T. Yamagata, H. Akimune, Y. Arimoto, H. Daito *et al.*, Phys. Rev. C **72**, 041001 (2005).
[23] S. Hilaire, M. Girod, S. Goriely, and A. J. Koning, Phys. Rev. C **86**, 064317 (2012).
[24] J. Kopecky (private communication).
[25] J. Kopecky and R. E. Chrien, Nucl. Phys. A **468**, 285 (1987).
[26] J. Kopecky and M. Uhl, Phys. Rev. C **41**, 1941 (1990).
[27] *Handbook for Calulations of Nuclear Reaction Data*, Reference Input Parameter Library, IAEA-Tecdoc-1034 (International Atomic Energy Agency, Vienna, 1998).
[28] R. Massarczyk, G. Rusev, R. Schwengner, F. Dönau, C. Bhatia, M. E. Gooden, J. H. Kelley, A. P. Tonchev, and W. Tornow, Phys. Rev. C **90**, 054310 (2014).
[29] R. M. Laszewski, R. Alarcon, and S. D. Hoblit, Phys. Rev. Lett. **59**, 431 (1987).
[30] R. M. Laszewski, P. Rullhusen, S. D. Hoblit, and S. F. LeBrun, Phys. Rev. C **34**, 2013(R) (1986).
[31] R. M. Laszewski, R. Alarcon, D. S. Dale, and S. D. Hoblit, Phys. Rev. Lett. **61**, 1710 (1988).
[32] R. Alarcon, R. M. Laszewski, and D. S. Dale, Phys. Rev. C **40**, R1097 (1989).
[33] A. Richter, A. Weiss, O. Haüsser, and B. A. Brown, Phys. Rev. Lett. **65**, 2519 (1990).
[34] D. Frekers *et al.*, Phys. Lett. B **244**, 178 (1990).
[35] N. Pietralla, P. von Brentano, R.-D. Herzberg, U. Kneissl, J. Margraf, H. Maser, H. H. Pitz, and A. Zilges, Phys. Rev. C **52**, R2317 (1995).
[36] C. Lüttge, P. von Neumann-Cosel, F. Neumeyer, C. Rangacharyulu, A. Richter, G. Schrieder, E. Spamer, D. I. Sober, S. K. Matthews, and B. A. Brown, Phys. Rev. C **53**, 127 (1996).
[37] C. Fransen, B. Krischok, O. Beck, J. Besserer, P. von Brentano, T. Eckert, R.-D. Herzberg *et al.*, Phys. Rev. C **59**, 2264 (1999).
[38] A. Linnemann, P. von Brentano, J. Eberth, J. Enders, A. Fitzler, C. Fransen *et al.*, Phys. Lett. B **554**, 15 (2003).
[39] A. S. Adekola, C. T. Angell, S. L. Hammond, A. Hill, C. R. Howell, H. J. Karwowski, J. H. Kelley, and E. Kwan, Phys. Rev. C **83**, 034615 (2011).
[40] W. Mettner, A. Richter, W. Stock, B. C. Metsch, and A. G. M. Van Hees, Nucl. Phys. A **473**, 160 (1987).
[41] N. Pietralla, P. von Brentano, R.-D. Herzberg, U. Kneissl, N. Lo Iudice, H. Maser, H. H. Pitz, and A. Zilges, Phys. Rev. C **58**, 184 (1998).
[42] R. Köhler, J. A. Wartena, H. Weigmann, L. Mewissen, F. Poortmans, J. P. Theobald, and S. Raman, Phys. Rev. C **35**, 1646 (1987).
[43] J. Birkhan, H. Matsubara, P. von Neumann-Cosel, N. Pietralla, V. Yu. Ponomarev, A. Richter, A. Tamii, and J. Wambach, Phys. Rev. C **93**, 041302(R) (2016).
[44] M. Guttormsen, L. A. Bernstein, A. Gorgen, B. Jurado, S. Siem *et al.*, Phys. Rev. C **89**, 014302 (2014).
[45] J. L. Ullmann, T. Kawano, T. A. Bredeweg, A. Couture, R. C. Haight, M. Jandel *et al.*, Phys. Rev. C **89**, 034603 (2014).
[46] S. Goriely, S. Hilaire, and A. J. Koning, Phys. Rev. C **78**, 064307 (2008).
[47] A. J. Koning, S. Hilaire, and S. Goriely, Nucl. Phys. A **810**, 13 (2008).
[48] S. Goriely, S. Hilaire, and A. J. Koning, Astron. Astrophys. **487**, 767 (2008)
[49] A. J. Koning, S. Hilaire, and M. C. Duijvestijn, in *Nuclear Data for Science and Technology*, edited by O. Bersillon *et al.* (EDP Sciences, Les Ulis, France, 2008), p. 211.
[50] A. J. Koning and D. Rochman, Nucl. Data Sheets **113**, 2841 (2012).